ACS OMEGA

http://pubs.acs.org/journal/acsodf

Article

Cross-Linked Composite Gel Polymer Electrolyte Based on an H-Shaped Poly(ethylene oxide)−Poly(propylene oxide) Tetrablock Copolymer with SiO_2 Nanoparticles for Solid-State Supercapacitor Applications

Sohee Kim, Ji Hee Kim, Jae Hee Han, Jang Yong Lee, Soonyong So, Sang Jun Yoon, Hyung-Joong Kim, Kyu Tae Lee,* and Tae-Ho Kim*

Cite This: *ACS Omega* 2021, 6, 16924−16933

Read Online

ACCESS | Metrics & More | Article Recommendations | Supporting Information

ABSTRACT: Achieving high ionic conductivity, wide voltage window, and good mechanical strength in a single material remains a key challenge for polymer-based electrolytes for use in solid-state supercapacitors (SCs). Herein, we report cross-linked composite gel polymer electrolytes (CGPEs) based on multi-cross-linkable H-shaped poly(ethylene oxide)−poly(propylene oxide) (PEO-PPO) tetrablock copolymer precursors, SiO_2 nanoparticles, and 1-ethyl-3-methylimidazolium bis(trifluoromethylsulfonyl)imide, an ionic liquid (IL). Self-standing CGPE membranes with a high IL content were prepared using in situ cross-linking reactions between the silane groups present in the precursor and the SiO_2 surface. The incorporation of an optimal amount of SiO_2 increased the cross-linking density of the resulting CGPE while reducing polymer-chain ordering and, consequently, increasing both ionic conductivity and mechanical strength. As a result, the CGPE with 0.1 wt % SiO_2 exhibited a high ionic conductivity (2.22×10^{-3} S cm^{-1} at 25 °C), good tensile strength (453 kPa), and high thermal stability up to 330 °C. Finally, an all-solid-state SC assembled with the prepared CGPE showed a high operating voltage (3 V), a large specific capacitance (103.9 F g^{-1} at 1 A g^{-1}), and excellent durability (94% capacitance retention over 10,000 charge/discharge cycles), which highlights its strong potential as a solid-state electrolyte for SCs.

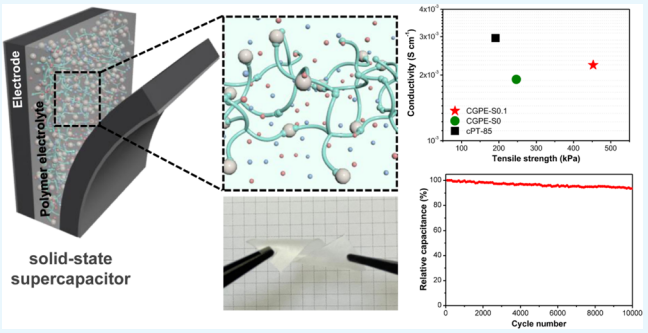

1. INTRODUCTION

Supercapacitors (SCs), also known as electric double-layer capacitors or ultracapacitors, are energy-storage devices that store and release electrical energy using the electric double-layer phenomenon at the interface between the electrode surface and the electrolyte. SCs using reversible ion adsorption have attractive properties, including high power densities, long cycle lives, cost effectiveness, and ecofriendliness.[1,2] However, SCs with conventional liquid electrolytes exhibit several stability issues, including battery stability and long-term operational stability, due to liquid leakage and corrosion problems.[3] To overcome these limitations, various polymer-based electrolytes have been studied as alternatives to liquid electrolytes.[4,5] The gel polymer electrolyte (GPE), which consists of a host polymer matrix and liquid electrolytes or ionic liquids (ILs), has a solid or semisolid phase, depending on the content of liquid composition. The advantages of a GPE, such as high ionic conductivity, flexibility, easy design configuration, and simple packaging, offer strong possibilities for applications in flexible or stretchable electronics.[6,7] In addition, GPEs with sufficient mechanical strengths not only act as electrolytes but can also act as the separators that prevent direct contact between electrodes.[8−10] Therefore, it is possible to reduce the resistance of an SC through the use of a thin self-standing GPE membrane and no separator.

In an IL-based GPE, the IL serves as both the ion source and the solvent. Due to the absence of a conventional organic solvent, IL-based GPEs possess excellent properties, including good electrochemical stability, wide voltage windows (>3 V), negligible vapor pressures, nonvolatility, and nonflammability.[11−13] In particular, since the energy density of an SC is proportional to the square of the voltage, IL-based GPEs are very advantageous for achieving SC devices with high energy densities. Nevertheless, ILs have relatively poor ionic conductivities and are highly viscous compared with conven-

Received: March 26, 2021
Accepted: June 11, 2021
Published: June 24, 2021

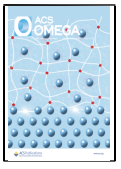

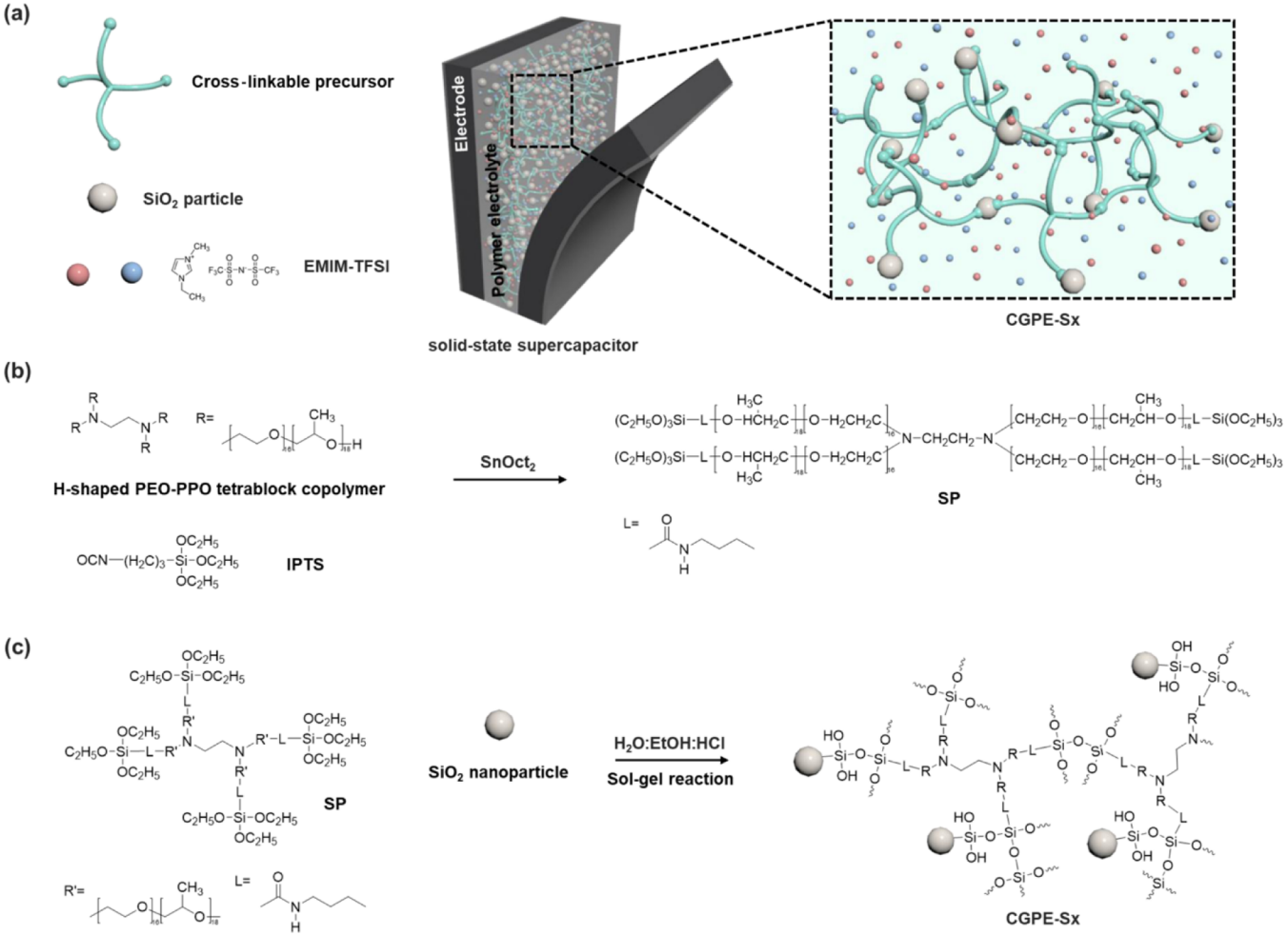

Figure 1. (a) Schematic illustration of the solid-state SC with CGPE and synthetic schemes of (b) SP and (c) CGPE-S*x*.

tional liquid electrolytes based on organic solvents, such as acetonitrile or propylene carbonate.[14−16] The IL content of the GPE should be as high as possible in order to achieve a sufficiently ionically conductive IL-based GPE; however, the mechanical strength of the GPE tends to be inversely proportional to the IL content. The GPE loses its mechanical integrity as a solid-state electrolyte and can no longer act as a separator when an excessive amount of an IL is included in the GPE. In this regard, it is very important to develop GPEs with balanced ionic conductivities and mechanical properties in which mechanical strength is maintained even at a high IL content.

Cross-linking provides an excellent solution to the above-mentioned issues. In particular, in situ cross-linkable GPEs, which are initially in the forms of non-cross-linked precursors that can be transformed into cross-linked structures during membrane fabrication, can solve the processability issues associated with other cross-linked GPEs.[17−19] We previously developed an in situ cross-linkable GPE composed of poly(ethylene oxide)−poly(propylene oxide)−poly(ethylene oxide) (PEO-PPO-PEO) triblock copolymer precursors with cross-linkable silane end groups and an IL.[20] The cross-linked GPE maintained its mechanical integrity and exhibited a well-balanced combination of a high ionic conductivity and good mechanical stability, even when 200% of the IL was included.

In this study, we developed in situ cross-linked composite GPEs (CGPEs) composed of a multifunctional H-shaped PEO-PPO tetrablock copolymer precursor, SiO_2 nanoparticles capable of bonding with the polymer matrix, and a high-voltage IL (Figure 1a). The multifunctional H-shaped precursor significantly improved the cross-linking density of the polymer matrix in the GPE by increasing the number of branch points in the cross-linked structure compared with conventional linear polymer matrixes. Moreover, the mechanical strength of the resulting GPE is further increased by incorporating SiO_2 nanoparticles, which become interlocked with the ends of the polymer matrix; the Si−OH groups on the SiO_2 surface form −Si−O−Si− linkages with the triethoxysilane end groups of the polymer matrix through sol−gel reactions. This distinguishes it from conventional composite GPEs. In our CGPEs, the SiO_2 nanoparticles can be uniformly dispersed and multiple covalent bonds can be formed between the nanoparticles and the polymer matrix.[21,22] Then, even if a small amount of SiO_2 nanoparticles are introduced, the mechanical strength of CGPE is improved, which can maximize the IL content. The CGPE containing 200% of the IL exhibited a high ionic conductivity (2.22×10^{-3} and 1.1×10^{-2} S cm^{-1} at 25 and 80 °C, respectively) and excellent mechanical strength (tensile strength of 453 kPa and maximum elongation of ∼65%). The electrochemical performance of a solid-state SC containing the CGPE was evaluated by electrochemical impedance spectroscopy (EIS), linear sweep voltammetry (LSV), cyclic voltammetry (CV), and galvanostatic charge−discharge (GCD) tests.

https://doi.org/10.1021/acsomega.1c01623
ACS Omega 2021, 6, 16924−16933

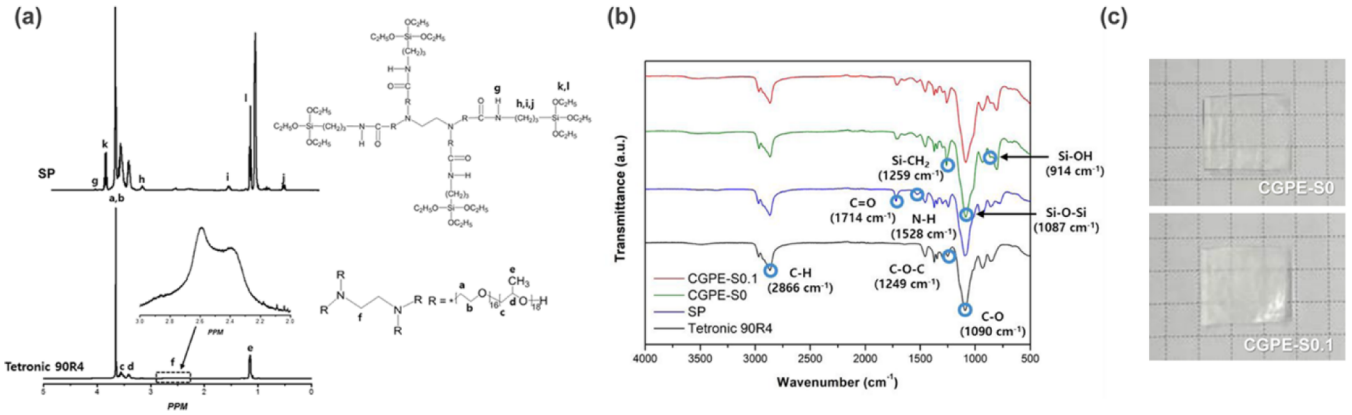

Figure 2. (a) ^{1}H NMR spectra of Tetronic 90R4 and SP. (b) FT-IR spectra of Tetronic 90R4, SP, CGPE-S0, and CGPE-S0.1 without IL, showing characteristic bands along with corresponding assignments. (c) Photographic images of the CGPE-S0 and CGPE-S0.1.

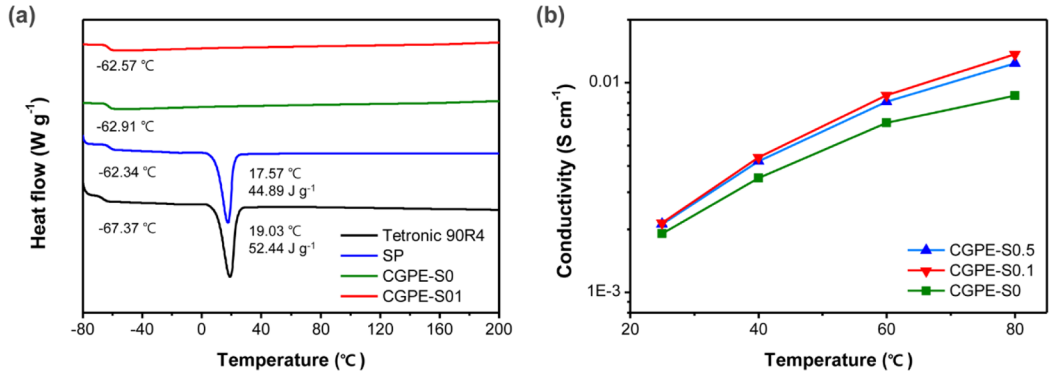

Figure 3. (a) DSC curves of Tetronic 90R4, SP, CGPE-S0, and CGPE-S0.1 without IL. (b) CGPE ionic conductivities as functions of temperature.

2. RESULTS AND DISCUSSION

2.1. Synthesis of SP and CGPEs. The overall pathway for the synthesis of SP and CGPEs is shown in Figure 1b,c. A triethoxysilane-end-capped PEO-PPO tetrablock precursor, SP, was prepared by condensation reactions of the terminal hydroxyl end groups of Tetronic 90R4 with 3-isocyanatopropyl triethoxysilane (IPTS). The resulting triethoxysilane end groups act as multi-cross-linkable units in the subsequent sol−gel reaction. SP was successfully synthesized, as confirmed by ^{1}H NMR and Fourier transform infrared (FT-IR) (Figure 2a,b, respectively). The ^{1}H NMR spectrum of SP shows peaks corresponding to N−H of urethane groups at 4.2 ppm and the ethoxy groups of the $-Si(OEt)_3$ at around 1.25 and 4.0 ppm. By comparing the integral value of the proton peaks of SP, it was confirmed that the silane end groups were introduced at the terminal of the tetrablock copolymer in almost 100% conversion. The FT-IR spectrum showed bands at 1528 and 1714 cm^{-1} that are attributable to the urethane bonds and at 1259 cm^{-1} that are due to the $-CH_2-Si$ groups. These results confirm that the hydroxyl end groups of the PEO-PPO tetra block precursor had been successfully converted into triethoxysilane groups.

The cross-linked GPEs were prepared using an in situ sol−gel cross-linking process accompanied by solvent evaporation from solutions containing SP and IL with and without SiO_2 nanoparticles. Through the sol−gel process, the trifunctional triethoxysilane end groups of SP react with each other to form a highly cross-linked structure. When SiO_2 nanoparticles are included in the reaction (as in CGPE-S0.1 and CGPE-S0.5), Si−O−Si groups are formed through condensation reactions between triethoxysilane end groups of the SP as well as between triethoxysilane groups of SP and the Si−OH groups on the surface of the SiO_2 nanoparticles. It has been well recognized that the addition of nanometer-sized ceramic fillers into polymer electrolyte enhances the interaction between the ceramic surface and the polymer chains.[25,26] For this reason, 50 nm-sized SiO_2 particles with a narrow size distribution were used in this study. The IR spectrum of CGPE-S0 (prepared without SiO_2 nanoparticles) shows a vibrational band at 1087 cm^{-1} that corresponds to the stretching vibrations of Si−O−Si groups, while the IR spectrum of CGPE-S0.1 shows a vibrational band of Si−O−Si groups (1087 cm^{-1}) and the vibrational bands of the remaining Si−OH groups (914 cm^{-1}) of the SiO_2 nanoparticles.

CGPE films were prepared using a solution casting method. While SP, the un-cross-linked precursor, exhibits as a paraffin-like phase at room temperature, all CGPE films are in the solid phase with good mechanical integrities, despite their high IL contents (200 wt %). Photographic images of 130 μm-thick CGPE-S0 and CGPE-S0.1 reveal that they are translucent, smooth, and devoid of any noticeable nanoparticle agglomeration (Figure 2c). Figure S2 shows the EDS mapping images for C, O, and Si elements of CGPE-S0 and CGPE-S0.1 There is no difference between the two films in terms of the kinds of constituent elements; C, O, and Si elements are commonly present in both films. However, for the image of CGPE-S0.1, spatially increased Si element content was observed in some areas, presenting the presence of SiO_2. Moreover, it was found that the SiO_2 nanoparticles are uniformly distributed over the entire film area.

https://doi.org/10.1021/acsomega.1c01623
ACS Omega 2021, 6, 16924−16933

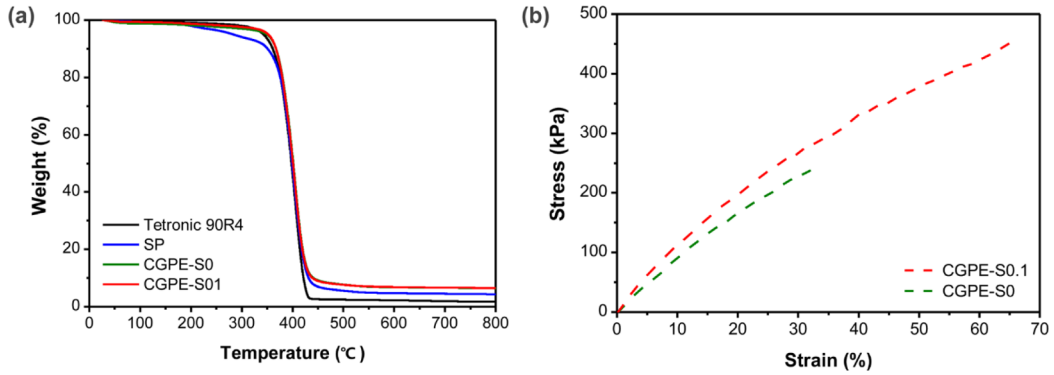

Figure 4. (a) TGA curves of Tetronic 90R4, SP, CGPE-S0, and CGPE-S0.1 without IL. (b) Stress−strain curves for CGPE-S0 and CGPE-S0.1.

2.2. Electrochemical Characterization. Among various polymer matrixes for GPEs, PEO is one of the most widely studied polymers because of its low lattice energy, good electrochemical stability, and ion-conducting ability.[27−29] However, PEO-based GPE systems suffer from low ionic conductivities at ambient temperature because PEO has a highly crystalline structure below its melting temperature (T_m).[17,30,31] However, for the CGPE-Sx in this study, the cross-linking reactions between the SP chain ends proceed in solution, which successfully inhibited PEO block crystallization in the SP.[22,32]

To examine the amorphousness of the cross-linked membrane, differential scanning calorimetry (DSC) of Tetronic 90R4, SP, CGPE-S0, and CGPE-S0.1 was performed from −80 to 200 °C. The second heating curves of all samples are shown in Figure 3a. Tetronic 90R4 and SP present strong endothermic peaks at 19.03 and 17.57 °C, respectively, which correspond to the T_ms of the crystalline domains in the polymer matrixes and indicate that the starting material (the PEO-PPO tetrablock copolymer) and the triethoxysilane end-capped precursor (SP) have a crystalline structure at room temperature. On the other hand, no endothermic T_m was observed up to 200 °C in the DSC curves of CGPE-S0 and CGPE-S0.1, which supports the notion that the CGPEs are completely amorphous, irrespective of the SiO_2 content. Nevertheless, it is important to note that CGPE-S0 and CGPE-S0.1 exhibited quite low T_gs of −62.91 and −62.57 °C, respectively, and these values are essentially the same as the T_g of the un-cross-linked SP precursor (−62.34 °C). Clearly, cross-linking the SP end groups hardly affects the flexibility of the resulting polymer network; the CGPEs are sufficiently highly flexible to allow segmental motion of the PEO chains necessary to mediate ionic conduction at room temperature.

The wide-angle X-ray diffraction (WAXD) patterns of SiO_2 nanoparticles, CGPE-S0, and CGPE-S0.1 are shown in Figure S3. Although PEO-PPO block copolymers were reported to have crystalline structures,[20,33] CGPE-S0 and CGPE-S0.1 did not have distinct peaks but showed only a broad amorphous halo in the pattern, confirming their complete amorphous structure.

The ionic conductivities of CGPE-S0, CGPE-S0.1, and CGPraE-S0.5 containing 1-ethyl-3-methylimidazolium bis-(trifluoromethylsulfonyl)imide (EMIM TFSI, 200 wt % with respect to polymer weight) were measured under non-humidified conditions in the 25−80 °C range, the results of which are shown in Figure 3b. All CGPEs exhibited ionic conductivities that increased with increasing temperature due to higher ion migration and greater segmental motions of polymer chains at elevated temperatures. The ionic conductivity of CGPE-S0 increased from 1.91×10^{-3} S cm^{-1} (25 °C) to 7×10^{-3} S cm^{-1} (80 °C). According to previous reports, conventional IL-containing PEO electrolytes exhibit poor mechanical properties (e.g., brittleness) and much lower ionic conductivity (10^{-4} to 10^{-5} S cm^{-1} at 25 °C) even at IL contents above 150 wt % due to their crystalline structures.[20,34,35] Note that the conductivity of CGPE-S0 is approximately 2 orders of magnitude higher than that of PEO at ambient temperature, which indicates that the amorphousness of CGPE-S0 created through in situ cross-linking successfully improves the ionic conductivity.

More interestingly, the addition of a small amount of SiO_2 nanoparticles further increased the ionic conductivity of CGPE; CGPE-S0.1 and CGPE-S0.5 exhibited ionic conductivities of 2.22×10^{-3} and 2.11×10^{-3} S cm^{-1}, respectively, at 25 °C, slightly higher than that of CGPE-S0. The ionic conductivities of the CGPEs with SiO_2 were further improved at higher temperatures, with values of 1.2×10^{-2} and 1.1×10^{-2} S cm^{-1} measured for CGPE-S0.1 and CGPE-S0.5, respectively, at 80 °C, which correspond to increases of 71 and 57%, respectively, over that of CGPE-S0. We believe that the small amount of the introduced inorganic particles act as cross-linking centers between polymers that further reduce polymer crystallinity and promote segmental motion.[31,36,37] Composite polymer electrolytes (CPEs) fabricated by adding inorganic particles, such as Al_2O_3, Fe_2O_3, MgO, SiO_2, and TiO_2, have been previously studied;[38−41] the addition of inorganic particles was observed to increase ionic conductivity by decreasing polymer crystallinity as well as improving the mechanical properties and thermal stability of the CPEs. Lin et al. also reported that inorganic particles added to a PEO matrix act like plasticizers that inhibit crystallization of the PEO chains and promote segmental motion of the polymers.[22] The ionic conductivity of CGPE slightly decreased as the amount of added SiO_2 was increased from 0.1 to 0.5 wt %, while the ionic conductivity of CGPE-S0.5 was still higher than that of CGPE-S0, which suggest that an optimum amount of SiO_2 nanoparticles exists in terms of ionic conductivity, with nanoparticles gradually beginning to block ion-transport pathways as this optimal value is exceeded.[40] Based on these ionic conductivity results, CGPE-S0.1 was used in the remaining investigations.

LSV measurement was performed to evaluate the electrochemical stability window of GCPE-S0.1. As can be seen in Figure S4, no significant increase in the current density was observed before 4.26 V. This result indicates that CGPE-S0.1 has sufficient electrochemical stability for use in SCs.

https://doi.org/10.1021/acsomega.1c01623
ACS Omega 2021, 6, 16924−16933

2.3. Thermal and Mechanical Stabilities. Figure 4a shows thermogravimetric analysis (TGA) curves of Tetronic 90R4, SP, CGPE-S0, and CGPE-S0.1 acquired in the 25−800 °C temperature range under nitrogen. Tetronic 90R4 underwent single-step decomposition from around 330 °C, while the SP precursor exhibited a two-step weight loss at around 200 and 330 °C; the first loss is likely due to the thermally initiated condensation between the triethoxysilane end groups of SP, and the second loss corresponding to decomposition of the polymer backbone. No significant weight loss was observed up to 330 °C in the TGA curves of CGPE-S0 and CGPE-S0.1, confirming that few triethoxysilane end groups from SP remain following completion of the in situ cross-linking process. The higher char yield of the CGPEs (∼8%) compared to that of Tetronic 90R4 (∼2%) is presumably due to the presence of residual silica-based materials. The degradation of CGPE-S0 and CGPE-S0.1 began at around 330 °C, which indicates that they are sufficiently thermally stable for use as a candidate for electrolytes in SCs at a wide range of operating temperatures.[42]

Figure 4b shows stress−strain curves of CGPE-S0 and CGPE-S0.1, which reveals that CGPE-S0 has a high tensile strength of 247 kPa despite the inclusion of a large amount (200 wt %) of EMIM-TFSI. The cross-linked GPE (referred as "cPT-85") based on a linear PEO-PPO-PEO triblock copolymer exhibited a tensile strength of 191 kPa under the same measuring conditions (Figure S5). Based on this comparison, we hypothesize that the high degree of cross-linking resulting from the use of the H-shaped precursor led to the higher mechanical strength of the CGPE compared to that of cPT-85. More interestingly, CGPE-S0.1, formed using a small amount of SiO_2 nanoparticles, not only exhibited an even higher tensile strength (453 kPa) than CGPE-S0 but also a larger elongation (65%). We believe that the formation of the polymer-matrix/SiO_2-nanoparticle network through chemical bonding further improves the mechanical properties of CGPE-S0.1.

To evaluate the balance between the ion-conducting and mechanical properties of the prepared GPEs, the results for CGPE-S0, CGPE-S0.1, cPT-85 and the recently reported PEO-based GPEs are summarized in Figure 5. The bare PEO with 1-butyl-3-methylimidazolium tetrafluoroborate (BMIM-BF_4) exhibited a high tensile strength of over 1900 kPa but showed a low ionic conductivity of 8.8 × 10^{-5} S cm^{-1}, confirming again that the PEO-based GPE system suffers from low ionic conductivity due to its highly crystalline structure at ambient temperature.[20] cPT-85 exhibits the highest ionic conductivity but the lowest tensile strength among the GPEs prepared in this study. Based on the results for CGPE-S0, we hypothesize that the use of the H-shaped precursor effectively increases the tensile strength of the resulting electrolyte, albeit while sacrificing its ion-conducting capability. Despite exhibiting a slightly lower (∼25%) ionic conductivity than cPT-85, the mechanical strength of CGPE-S0.1 was more than twice that of cPT-85. As a result, we confirmed that the properties of CGPE-S0.1 are the best balanced in terms of performance and stability tradeoffs. The cross-linked PEO-based GPEs in the recent literature, including PEO-based epoxy resin/EMIM-TFSI[43] and PPO-PEO-PPO/EMIM-TFSI,[44] exhibited similar or higher ionic conductivities than CGPE-S0.1; however, their tensile strength values were still much lower than CGPE-S0.1. These results highlight the benefit of the material design strategy that employs both cross-linking and an organic−inorganic composite.[22,45,46]

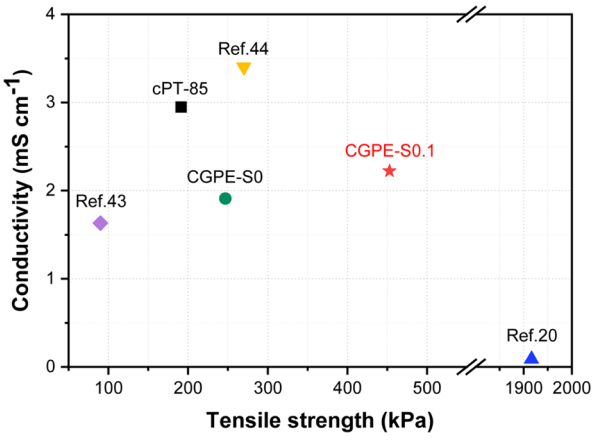

Figure 5. Comparison of balance between ionic conductivity and tensile strength of CGPE-S0, CGPE-S0.1, cPT-85, and other GPEs in the recent literature including PEO/BMIM-BF_4 (IL contents: 100 wt %),[20] PEO-based epoxy resin/EMIM-TFSI (IL contents: 200 wt %),[43] and PPO-PEO-PPO/EMIM-TFSI (IL contents: 70 wt %).[44]

2.4. Electrochemical Performance of the SC_CGPEs. The electrochemical performance of SC_CGPEs were evaluated by EIS, CV, and GCD testing at room temperature. Note that the CGPEs in this study are free-standing solid-phase electrolytes that do not require the use of an additional porous separator for the SC fabrication due to their sufficiently high mechanical strengths, as detailed above. EIS was used to study the resistance behavior and properties of the interface between activated carbon-based electrodes and the CGPE, with corresponding Nyquist plots shown in Figure 6a. The Nyquist plots of both SC_CGPE-S0 and SC_CGPE-S0.1 show semicircles in the high-frequency region and steeply increasing vertical lines in the low-frequency region. The intercept at the real axis in the high-frequency region reveals the equivalent series resistance (ESR), which is related to the resistance of the bulk electrolyte and the interfacial properties. The diameter of the depressed semicircle provides the interfacial resistance (R_{ct}) between the electrolyte and the electrode associated with charge transport. SC_CGPE-S0.1 exhibited a lower ESR value (3.11 Ω) than SC_CGPE-S0 (3.81 Ω), which indicates that SC_CGPE-S0.1 has a lower bulk resistance. Moreover, a somewhat smaller R_{ct} value was determined for SC_CGPE-S0.1 (1.15 Ω) compared to SC_CGPE-S0 (1.28 Ω), which is attributable to the higher ionic conductivity of SC_CGPE-S0.1, as revealed above.

Figure 6b shows CV profiles in the 0−3 V voltage range at a scan rate of 10 mV s^{-1}. The overall CV profiles at various scan rates (10, 20, 50, and 100 mV s^{-1}) are shown in Figure S6. No distinct peaks were observed in the CV curves at various scan rates, which are all nearly rectangular in shape, characteristic of typical electrochemical capacitors. These results indicate that no electron-transfer process or redox reaction occurs in the measured voltage range, confirming the absence of side reactions for SC_CGPE-S0 and SC_CGPE-S0.1. The CV curves for SC_CGPE-S0 and CGPE-S0.1 maintained their rectangular shapes even at a high scan rate of 100 mV s^{-1} (Figure 6c), suggestive of good rate capabilities. In addition, SC_CGPE-S0.1 exhibited a larger CV area than SC_CGPE-S0, which reveals that it has a higher specific capacitance.

The SCs were subjected to GCD testing in the wide 0−3 V voltage range at various current densities in the 0.1−10 A g^{-1}

https://doi.org/10.1021/acsomega.1c01623
ACS Omega 2021, 6, 16924−16933

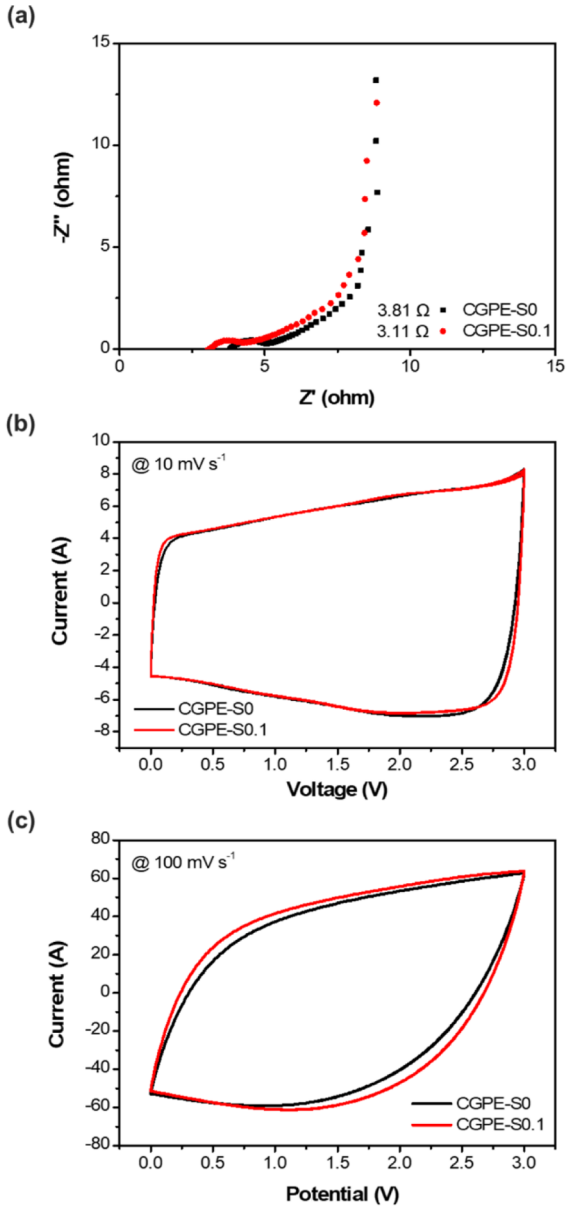

Figure 6. Electrochemical performance of SC_CGPE-S0 and SC_CGPE-S0.1. (a) Nyquist plots and CV curves at scan rates of: (b) 10 and (c) 100 mV s^{-1}.

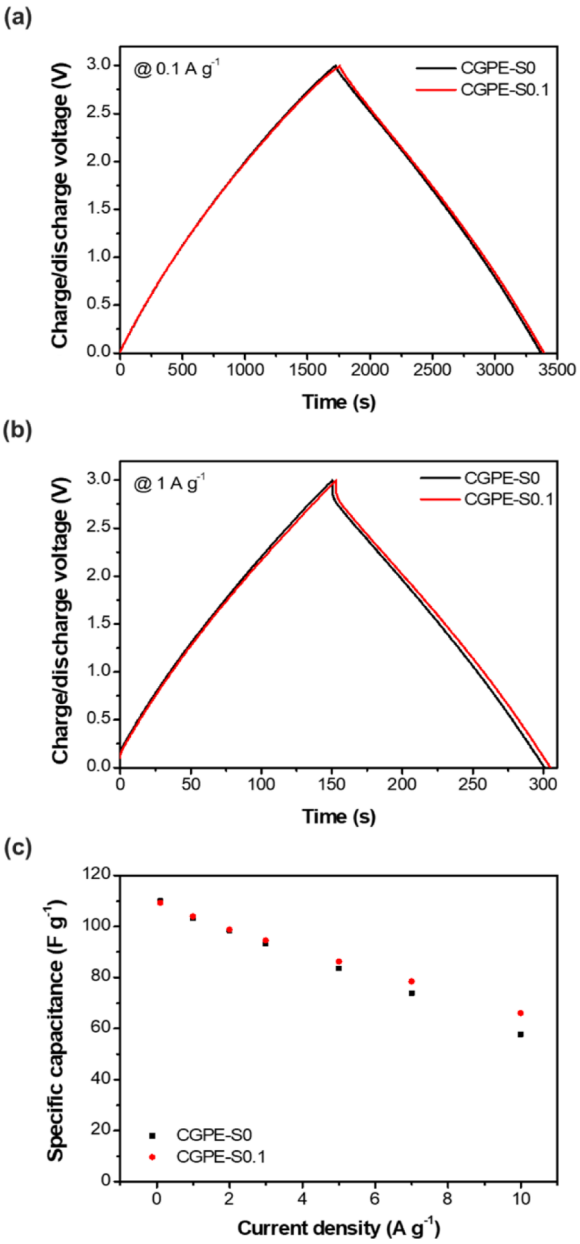

Figure 7. Comparative electrochemical performance of SC_CGPE-S0 and SC_CGPE-S0.1. GCD curves at current densities of: (a) 0.1 and (b) 1 A g^{-1}. (c) Specific capacitances at various current densities between 0.1 and 10 A g^{-1}.

range, the results of which are shown in Figures 7 and S3. The C_s values of the SCs, determined from the GCD curves using eq 1, are plotted as functions of current density in Figure 7c. Charging and discharging occurred quite reversibly for SC_CGPE-S0 and SC_CGPE-S0.1 at low current densities, such as 0.1 and 1 A g^{-1}, with typical triangular electrical double-layer capacitor GCD curves observed (Figure 7a,b). The capacitances of the SC_CGPE-S0 were calculated to be 109.92 and 103.11 F g^{-1} at current densities of 0.1 A, respectively, which are almost identical to those of SC_CGPE-S0.1 (109.24 and 103.90 F g^{-1}). As both CGPE-S0 and CGPE-S0.1 possess sufficient ionic conductivities, their capacitive performance at a slow charge−discharge rate mainly depends on the performance of the electrode. However, the C_s of SC_CGPE-S0 and SC_CGPE-S0.1 gradually decreased with increasing applied current density to 10 A g^{-1}, most probability due to ion-diffusion limitations in the GPEs. Nevertheless, the capacity retention of SC_CGPE-S0.1 at 10 A g^{-1} was 60.49% with respect to the initial capacity at 0.1 A g^{-1}, while that of SC_CGPE-S0 was 52.56% under the same conditions. Considering that the loading density of each electrode is high (6.0−6.8 mg cm^{-2}), the measured rate capabilities of the SC_CGPEs seem reasonable. The IR drop in the initial part of each discharge slope is associated with the overall ESR of the device. As shown in Figure 7b (at 1 A g^{-1}) and Figure S7 (at 10 A g^{-1}), SC_CGPE-S0.1 exhibited smaller R_{ESR} values than SC_CGPE-S0. The R_{ESR} values of the SC_CGPEs were calculated from their GCD profiles using eq 2, which revealed that the R_{ESR} of SC_CGPE-S0.1 (5.27 Ω cm^2) is lower than that of SC_CGPE-S0 (5.53 Ω cm^2) at 1 A g^{-1}, which is in good agreement with the impedance results discussed above. Thus, SC_CGPE-S0.1 exhibited a higher specific capacitance

https://doi.org/10.1021/acsomega.1c01623
ACS Omega 2021, 6, 16924−16933

at a higher current density (i.e., better rate performance) than SC_CGPE-S0.

Specific energy densities (E_s) and power densities (P_s) were calculated from the GCD profiles according to eqs 3 and 4. As shown in Table S1, CGPE-S0.1 delivered an E_s of 30.83 W h kg^{-1} and a P_s of 1.461 kW kg^{-1} at 1 A g^{-1}, which are similar to those of CGPE-S0 (E_s = 30.50 W h kg^{-1}; P_s = 1.459 kW kg^{-1}). However, at 10 A g^{-1}, the differences in the E_s and P_s values of CGPE-S0 and CGPE-S0.1 were larger, with values of 11.12 W h kg^{-1} and 11.263 kW kg^{-1} for CGPE-S0 and 12.04 W h kg^{-1} and 11.473 kW kg^{-1} for CGPE-S0.1, respectively. Given that the manufactured device is an all-solid-state SC, we believe that these values are reasonable from a practical point of view.[47] In addition, the cycling stability of SC_CGPE-S0.1 and SC_CGPE-S0 was evaluated through continuous GCD cycling at 0−3 V and 10 A g^{-1} for 10,000 cycles. Figure 8 shows that

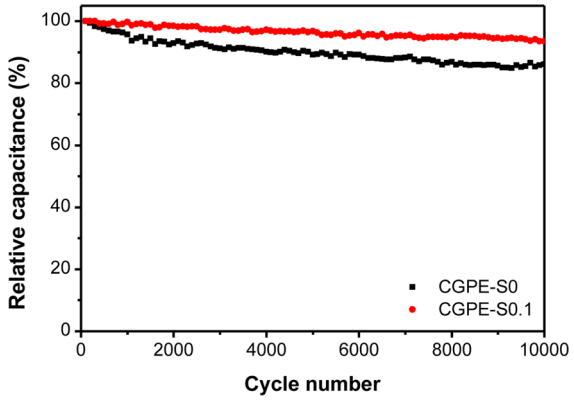

Figure 8. Cycling performance profiles of SC_CGPE-S0 and SC_CGPE-S0.1 at a current density of 10 A g^{-1}.

SC_CGPE-S0.1 retained 94% of its capacitance after 10,000 cycles, which highlights the excellent electrochemical stability of SC_CGPE-S0.1 during long-term cycling. SC_CGPE-S0 also exhibited a stable cycling profile, while the capacitance retention after 10,000 cycles is 86.13%, which is slightly lower than that of SC_CGPE-0.1. We believe the somewhat inferior conducting capability of CGPE-S0 than CGPE-S0.1 may be the reason for the lower retention rate.

3. CONCLUSIONS

We developed cross-linked composite GPEs (CGPEs) using an H-shaped PEO-PPO tetrablock copolymer precursor with cross-linkable triethoxysilane end groups, SiO_2 nanoparticles, and an IL (EMIM-TFSI). The in situ cross-linked structure formed through sol−gel reactions between the precursor end groups as well as the precursor and the SiO_2 nanoparticles resulted in greatly improved CGPE mechanical properties. Consequently, the prepared CGPEs maintained a solid phase when a large amount of IL was used and exhibited a high tensile strength that exceeded 400 kPa at an IL content of 200 wt %. Therefore, the CGPE formed with 0.1 wt % SiO_2 exhibited well-balanced electrolyte properties, presenting both high ionic conductivity (2.22 × 10^{-3} S cm^{-1}) at room temperature and good mechanical stability. The SC assembled with CGPE-S0.1 (SC_CGPE-S0.1) exhibited a high specific capacitance (109.24 F g^{-1} at 0.1 A g^{-1}), excellent rate capability (60.49% capacity retention to 10 A g^{-1}), and good durability (94% capacitance retention over 10,000 charge/discharge cycles). These results suggest that SC_CGPE-S0.1 is a suitable candidate for all solid-state SC applications.

4. MATERIALS AND METHODS

4.1. Materials. Ethylenediamine tetrakis(ethoxylate-*block*-propoxylate) tetrol (Tetronic 90R4, M_n ∼ 8000 g mol^{-1}), stannous 2-ethyl-hexanoate ($SnOct_2$, 98%), IPTS (95%), *N*-methyl-2-pyrrolidone (NMP), chloroform, and methanol were purchased from Sigma-Aldrich (USA). EMIM-TFSI 99% was purchased from C-TRI (South Korea). Petroleum ether (95%) was purchased from Samchun (South Korea). Silicon dioxide (SiO_2, 50 nm) particles was purchased from Sukgyung AT co. Prior to use, the Tetronic 90R4 and SiO_2 particles were dried under vacuum conditions at 80 °C for 24 h. Other reagents used in this work were used as received without any further purification.

4.2. Synthesis of the Triethoxysilane-End-Capped PEO-PPO Precursor (SP). Vacuum-dried Tetronic 90R4 (5 g, 1 mol), IPTS (0.72 g, 4 mol), and $SnOct_2$ (0.08 g, 3 mol) were placed in a three-necked flask and mixed with a magnetic stirrer in an argon atmosphere for around 1 h at 75 °C. The mixture was diluted in chloroform and precipitated in cold petroleum ether; then, petroleum ether was removed to obtain a viscous yellow liquid. Finally, the resultant viscous yellow liquid was dried in a vacuum oven at room temperature for 24 h. The precursor with triethoxysilane-end-capped PEO-PPO tetrablock copolymer was named "SP".

4.3. Preparation of the GPEs. The GPEs with a film form were obtained through a simple casting and thermal cross-linking method accompanying the sol−gel reaction. SP was dissolved in methanol (8 wt %), and the resulting solution was added with EMIM-TFSI (200 wt %) and sonicated for 30 min. Then the solution was added with water/EtOH/HCl (1:3.2:0.13, v/v) mixture and sonicated for an additional 30 min. The resulting IL-SP solution was filtered through a 0.45 μm Teflon syringe filter. In the cases of GPEs incorporating SiO_2, proper contents (0, 0.1, and 0.5 wt %) of SiO_2 particles were added to the prepared IL-SP/SiO_2 solution and the mixture solution was then sonicated for 30 min to obtain well-dispersed SiO_2 particles. The mixture solutions were casted on a Teflon sheet and thermally cross-linked using a halogen lamp at 60 °C for 6 h under a nitrogen atmosphere and then vacuum-dried at 40 °C for 24 h to remove the residual solvent. The resulting CGPE is named "CGPE-S*x*", where S means SiO_2 and *x* indicates the weight percentage of the SiO_2 particles with respect to the weight of the SP. The CGPE-Ss were punched into 16.0 mm pieces prior to use and the thickness of CGPEs was around 130 μm.

4.4. Preparation of Activated Carbon/Conductive Carbon Electrodes and Fabrication of SC Cells. The electrode used in the SC cell was manufactured as follows. The carbon electrodes were prepared by mixing activated carbon (YP50, 80 wt %), conducting carbon (Super P, 10 wt %) and binder (poly(vinylidene difluoride), 10 wt %) in NMP. The slurry was coated on the Al-foil sheet using a doctor blade and vacuum-dried at 80 °C for 2 days. The loading mass of each electrode was around 6.0−6.5 mg cm^{-2}. The SC cells were assembled using CR2032-type coin cells with two symmetrical carbon electrodes sandwiching CGPEs. The assembled SC cells were named "SC_CGPEs".

4.5. Characterization. The ^{1}H nuclear magnetic resonance (NMR, DPX-300, 300 MHz, Bruker) and FT-IR (ALPHA-P and ALPHA-T, Bruker) were used to investigate

https://doi.org/10.1021/acsomega.1c01623
ACS Omega 2021, 6, 16924−16933

the chemical structure. The morphologies of SiO_2 nanoparticles and CGPEs were observed using field-emission scanning electron microscopy (SEM, MIRA3 LMU, TESCAN) and energy-dispersive X-ray spectroscopy (EDS, Xflash FlatQUAD, Bruker) mapping. WAXD patterns of SiO_2 nanoparticles and CGPEs were recorded using a diffractometer (SmartLab, Rigaku) with Cu Kα radiation in the 2θ range of 10−60°. The thermal properties of CGPEs were evaluated by TGA (Pyris 1 PerkinElmer) and DSC (Q 1000, TA Instruments). TGA was carried out from room temperature to 800 °C under nitrogen flow at a heating rate of 10 °C min^{-1}, and DSC was employed to observe the thermal stability of CGPEs by temperature scan with a heating rate of 10 °C min^{-1} under a nitrogen atmosphere from −80 to 200 °C. The tensile strength, elongation, and Young's modulus of the CGPEs were measured using the universal tensile testing machine (Lloyd-Instruments calibration instrument, AMETEK) at room temperature with a gauge length of 200 mm and a 100 N load cell at a cross-head speed of 5 mm min^{-1}. The ionic conductivity (σ) of CGPEs was determined by EIS measurement in the frequency range from 4 MHz to 3 Hz under a nitrogen atmosphere at 25 and 80 °C using a SP-300 (BioLogic Science Instruments, France). The LSV was measured with two stainless-steel electrodes as the working and counter/reference electrodes. The voltage scan rate was 1 mV s^{-1} in the potential range from 2 to 5 V. The EIS measurements were carried out in a frequency range from 100 kHz to 10 mHz with an amplitude of the sinusoidal voltage of 10 mV. The CV tests of the SCs were conducted in a voltage range of 0 to 3 V at a different scan rates of 10, 20, 50, and 100 mV s^{-1}. The GCD tests were performed at the potential of 0 to 3 V at various current densities from 0.1 to 10 A g^{-1}. For all the electrochemical studies, a Biologic SP-300 electrochemical workstation was used.

4.6. Calculations of the Electrochemical Parameters. According to the GCD curves, the galvanostatic specific capacitance (C_s, in F g^{-1}) was calculated using the following equation[23]

$$C_s = 4I/[(\Delta V/\Delta t)m] \quad (1)$$

where I is the applied current (A), $\Delta V/\Delta t$ (in V s^{-1}) is the slope of the discharge curve after the initial IR drop, and m is the total mass (g) of two electrodes. The internal resistance was computed from the voltage drop at the beginning of each discharge[24]

$$R_{ESR} = \Delta V_{iR}/2i \quad (2)$$

where ΔV_{iR} and i are the voltage drops between the first two points in the voltage drop at the top cutoff and applied current, respectively.

The specific energy density (E_s, in W h kg^{-1}) and specific power density (P_s, in W kg^{-1}) were calculated according to

$$E_s = 0.5C_s(\Delta V)^2/3600M \quad (3)$$

$$P_s = E_s/\Delta t \quad (4)$$

where ΔV, Δt, and M are the potential window obtained from the discharge curve after the IR drop, discharge time, and the mass of electrodes (in kg), respectively.

■ ASSOCIATED CONTENT

Supporting Information

The Supporting Information is available free of charge at https://pubs.acs.org/doi/10.1021/acsomega.1c01623.

SEM image of SiO_2 nanoparticles; EDS mapping images of CGPE-S0 and CGPE-S0.1; WAXD patterns of SiO_2 nanoparticles, CGPE-S0, and CGPE-S0.1; LSV plot of CGPE-S0.1; stress−strain curve for cPT-85; CV curves for SC_CGPE-S0 and SC_CGPE-S0.1 at various scan rates; GCD curves for SC_CGPE-S0 and SC_CGPE-S0.1 at a current density of 10 A g^{-1}; ESRs, specific capacitances, power densities, and energy densities of the SC_CPGE-Ss at 1 A g^{-1} (PDF)

■ AUTHOR INFORMATION

Corresponding Authors

Kyu Tae Lee − *School of Chemical and Biological Engineering, Institute of Chemical Processes, Seoul National University, Seoul 08826, Republic of Korea;* orcid.org/0000-0003-2769-3372; Phone: +82-2-880-9394; Email: ktlee@snu.ac.kr

Tae-Ho Kim − *Energy Materials Research Center, Korea Research Institute of Chemical Technology, Daejeon 34114, Republic of Korea;* orcid.org/0000-0002-2130-9184; Phone: +82-42-860-7379; Email: thkim@krict.re.kr

Authors

Sohee Kim − *Energy Materials Research Center, Korea Research Institute of Chemical Technology, Daejeon 34114, Republic of Korea; School of Chemical and Biological Engineering, Institute of Chemical Processes, Seoul National University, Seoul 08826, Republic of Korea*

Ji Hee Kim − *Energy Materials Research Center, Korea Research Institute of Chemical Technology, Daejeon 34114, Republic of Korea; Department of Advanced Materials Engineering, Kongju National University, Cheonan 331-240, Republic of Korea*

Jae Hee Han − *Energy Materials Research Center, Korea Research Institute of Chemical Technology, Daejeon 34114, Republic of Korea*

Jang Yong Lee − *Energy Materials Research Center, Korea Research Institute of Chemical Technology, Daejeon 34114, Republic of Korea;* orcid.org/0000-0003-1996-1832

Soonyong So − *Energy Materials Research Center, Korea Research Institute of Chemical Technology, Daejeon 34114, Republic of Korea;* orcid.org/0000-0001-8677-7731

Sang Jun Yoon − *Energy Materials Research Center, Korea Research Institute of Chemical Technology, Daejeon 34114, Republic of Korea;* orcid.org/0000-0002-9159-2501

Hyung-Joong Kim − *Department of Advanced Materials Engineering, Kongju National University, Cheonan 331-240, Republic of Korea*

Complete contact information is available at: https://pubs.acs.org/10.1021/acsomega.1c01623

Author Contributions

S.K. and J.H.K. contributed equally. The manuscript was written through contributions of all authors. All authors have given approval to the final version of the manuscript.

Notes

The authors declare no competing financial interest.

■ ACKNOWLEDGMENTS

This work was supported by the Program through the National Research Foundation of Korea (NRF) Grant funded by the Korean government (sub no. 2020M3H4A3105818) and the Korea Research Institute of Chemical Technology (KRICT) core project (KS2122-10).

■ REFERENCES

(1) Wang, M.; Fan, L.; Qin, G.; Hu, X.; Wang, Y.; Wang, C.; Yang, J.; Chen, Q. Flexible and low temperature resistant semi-IPN network gel polymer electrolyte membrane and its application in supercapacitor. *J. Membr. Sci.* **2020**, *597*, 117740.

(2) Yong, H.; Park, H.; Jung, C. Quasi-solid-state gel polymer electrolyte for a wide temperature range application of acetonitrile-based supercapacitors. *J. Power Sources* **2020**, *447*, 227390.

(3) Jinisha, B.; Anilkumar, K. M.; Manoj, M.; Ashraf, C. M.; Pradeep, V. S.; Jayalekshmi, S. Solid-state supercapacitor with impressive performance characteristics, assembled using redox-mediated gel polymer electrolyte. *J. Solid State Electrochem.* **2019**, *23*, 3343−3353.

(4) Huang, Y.; Zhong, M.; Shi, F.; Liu, X.; Tang, Z.; Wang, Y.; Huang, Y.; Hou, H.; Xie, X.; Zhi, C. An Intrinsically Stretchable and Compressible Supercapacitor Containing a Polyacrylamide Hydrogel Electrolyte. *Angew. Chem., Int. Ed.* **2017**, *56*, 9141−9145.

(5) Genovese, M.; Wu, H.; Virya, A.; Li, J.; Shen, P.; Lian, K. Ultrathin all-solid-state supercapacitor devices based on chitosan activated carbon electrodes and polymer electrolytes. *Electrochim. Acta* **2018**, *273*, 392−401.

(6) Jin, M.; Zhang, Y.; Yan, C.; Fu, Y.; Guo, Y.; Ma, X. High-Performance Ionic Liquid-Based Gel Polymer Electrolyte Incorporating Anion-Trapping Boron Sites for All-Solid-State Supercapacitor Application. *ACS Appl. Mater. Interfaces* **2018**, *10*, 39570−39580.

(7) Yadav, N.; Yadav, N.; Hashmi, S. A. Ionic liquid incorporated, redox-active blend polymer electrolyte for high energy density quasi-solid-state carbon supercapacitor. *J. Power Sources* **2020**, *451*, 227771.

(8) Alexandre, S. A.; Silva, G. G.; Santamaría, R.; Trigueiro, J. P. C.; Lavall, R. L. A highly adhesive PIL/IL gel polymer electrolyte for use in flexible solid state supercapacitors. *Electrochim. Acta* **2019**, *299*, 789−799.

(9) Tiruye, G. A.; Muñoz-Torrero, D.; Palma, J.; Anderson, M.; Marcilla, R. Performance of solid state supercapacitors based on polymer electrolytes containing different ionic liquids. *J. Power Sources* **2016**, *326*, 560−568.

(10) Pandey, G. P.; Liu, T.; Hancock, C.; Li, Y.; Sun, X. S.; Li, J. Thermostable gel polymer electrolyte based on succinonitrile and ionic liquid for high-performance solid-state supercapacitors. *J. Power Sources* **2016**, *328*, 510−519.

(11) Gupta, A.; Jain, A.; Tripathi, S. K. Structural and electrochemical studies of bromide derived ionic liquid-based gel polymer electrolyte for energy storage application. *J. Energy Storage* **2020**, *32*, 101723.

(12) Poochai, C.; Sriprachuabwong, C.; Sodtipinta, J.; Lohitkarn, J.; Pasakon, P.; Primpray, V.; Maeboonruan, N.; Lomas, T.; Wisitsoraat, A.; Tuantranont, A. Alpha-MnO_2 nanofibers/nitrogen and sulfur-co-doped reduced graphene oxide for 4.5 V quasi-solid state supercapacitors using ionic liquid-based polymer electrolyte. *J. Colloid Interface Sci.* **2021**, *583*, 734−745.

(13) Zhang, J.; Sun, J.; Hu, Y.; Wang, D.; Cui, Y. Electrochemical capacitive properties of all-solid-state supercapacitors based on ternary MoS_2/CNTs-MnO_2 hybrids and ionic mixture electrolyte. *J. Alloys Compd.* **2019**, *780*, 276−283.

(14) Duay, J.; Gillette, E.; Liu, R.; Lee, S. B. Highly flexible pseudocapacitor based on freestanding heterogeneous MnO_2/conductive polymer nanowire arrays. *Phys. Chem. Chem. Phys.* **2012**, *14*, 3329−3337.

(15) Huang, C.-W.; Wu, C.-A.; Hou, S.-S.; Kuo, P.-L.; Hsieh, C.-T.; Teng, H. Gel Electrolyte Derived from Poly(ethylene glycol) Blending Poly(acrylonitrile) Applicable to Roll-to-Roll Assembly of Electric Double Layer Capacitors. *Adv. Funct. Mater.* **2012**, *22*, 4677−4685.

(16) Hu, X.-L.; Hou, G.-M.; Zhang, M.-Q.; Rong, M.-Z.; Ruan, W.-H.; Giannelis, E. P. A new nanocomposite polymer electrolyte based on poly(vinyl alcohol) incorporating hypergrafted nano-silica. *J. Mater. Chem.* **2012**, *22*, 18961−18967.

(17) Yu, Q.; Lu, Q.; Qi, X.; Zhao, S.; He, Y.-B.; Liu, L.; Li, J.; Zhou, D.; Hu, Y.-S.; Yang, Q.-H.; Kang, F.; Li, B. Liquid electrolyte immobilized in compact polymer matrix for stable sodium metal anodes. *Energy Storage Mater.* **2019**, *23*, 610−616.

(18) Zheng, J.; Yang, Y.; Li, W.; Feng, X.; Chen, W.; Zhao, Y. Novel flame retardant rigid spirocyclic biphosphate based copolymer gel electrolytes for sodium ion batteries with excellent high-temperature performance. *J. Mater. Chem. A* **2020**, *8*, 22962−22968.

(19) Yao, Y.; Wei, Z.; Wang, H.; Huang, H.; Jiang, Y.; Wu, X.; Yao, X.; Wu, Z. S.; Yu, Y. Toward High Energy Density All Solid-State Sodium Batteries with Excellent Flexibility. *Adv. Energy Mater.* **2020**, *10*, 1903698.

(20) Han, J. H.; Lee, J. Y.; Suh, D. H.; Hong, Y. T.; Kim, T.-H. Electrode-Impregnable and Cross-Linkable Poly(ethylene oxide)−Poly(propylene oxide)−Poly(ethylene oxide) Triblock Polymer Electrolytes with High Ionic Conductivity and a Large Voltage Window for Flexible Solid-State Supercapacitors. *ACS Appl. Mater. Interfaces* **2017**, *9*, 33913−33924.

(21) Depre, L.; Kappel, J.; Popall, M. Inorganic−organic proton conductors based on alkylsulfone functionalities and their patterning by photoinduced methods. *Electrochim. Acta* **1998**, *43*, 1301−1306.

(22) Lin, D.; Liu, W.; Liu, Y.; Lee, H. R.; Hsu, P.-C.; Liu, K.; Cui, Y. High Ionic Conductivity of Composite Solid Polymer Electrolyte via In Situ Synthesis of Monodispersed SiO_2 Nanospheres in Poly(ethylene oxide). *Nano Lett.* **2016**, *16*, 459−465.

(23) Song, S.; Ma, F.; Wu, G.; Ma, D.; Geng, W.; Wan, J. Facile self-templating large scale preparation of biomass-derived 3D hierarchical porous carbon for advanced supercapacitors. *J. Mater. Chem. A* **2015**, *3*, 18154−18162.

(24) Kim, M. S.; Hsia, B.; Carraro, C.; Maboudian, R. Flexible micro-supercapacitors with high energy density from simple transfer of photoresist-derived porous carbon electrodes. *Carbon* **2014**, *74*, 163−169.

(25) Liu, Y.; Lee, J. Y.; Hong, L. Functionalized SiO_2 in poly(ethylene oxide)-based polymer electrolytes. *J. Power Sources* **2002**, *109*, 507−514.

(26) Kim, H.-S.; Kum, K.-S.; Cho, W.-I.; Cho, B.-W.; Rhee, H.-W. Electrochemical and physical properties of composite polymer electrolyte of poly(methyl methacrylate) and poly(ethylene glycol diacrylate). *J. Power Sources* **2003**, *124*, 221−224.

(27) Singh, M.; Odusanya, O.; Wilmes, G. M.; Eitouni, H. B.; Gomez, E. D.; Patel, A. J.; Chen, V. L.; Park, M. J.; Fragouli, P.; Iatrou, H.; Hadjichristidis, N.; Cookson, D.; Balsara, N. P. Effect of Molecular Weight on the Mechanical and Electrical Properties of Block Copolymer Electrolytes. *Macromolecules* **2007**, *40*, 4578−4585.

(28) Bouchet, R.; Maria, S.; Meziane, R.; Aboulaich, A.; Lienafa, L.; Bonnet, J.-P.; Phan, T. N. T.; Bertin, D.; Gigmes, D.; Devaux, D.; Denoyel, R.; Armand, M. Single-ion BAB triblock copolymers as highly efficient electrolytes for lithium-metal batteries. *Nat. Mater.* **2013**, *12*, 452.

(29) Lehmann, M. L.; Yang, G.; Gilmer, D.; Han, K. S.; Self, E. C.; Ruther, R. E.; Ge, S.; Li, B.; Murugesan, V.; Sokolov, A. P.; Delnick, F. M.; Nanda, J.; Saito, T. Tailored crosslinking of Poly(ethylene oxide) enables mechanical robustness and improved sodium-ion conductivity. *Energy Storage Mater.* **2019**, *21*, 85−96.

(30) Nunes-Pereira, J.; Costa, C. M.; Lanceros-Méndez, S. Polymer composites and blends for battery separators: State of the art, challenges and future trends. *J. Power Sources* **2015**, *281*, 378−398.

(31) Tan, G.; Wu, F.; Zhan, C.; Wang, J.; Mu, D.; Lu, J.; Amine, K. Solid-State Li-Ion Batteries Using Fast, Stable, Glassy Nanocomposite Electrolytes for Good Safety and Long Cycle-Life. *Nano Lett.* **2016**, *16*, 1960−1968.

https://doi.org/10.1021/acsomega.1c01623
ACS Omega 2021, 6, 16924−16933

(32) Croce, F.; Persi, L.; Scrosati, B.; Serraino-Fiory, F.; Plichta, E.; Hendrickson, M. A. Role of the ceramic fillers in enhancing the transport properties of composite polymer electrolytes. *Electrochim. Acta* **2001**, *46*, 2457−2461.
(33) Larrañeta, E.; Isasi, J. R. Non-covalent hydrogels of cyclodextrins and poloxamines for the controlled release of proteins. *Carbohydr. Polym.* **2014**, *102*, 674−681.
(34) Ketabi, S.; Lian, K. Effect of SiO_2 on conductivity and structural properties of PEO−$EMIHSO_4$ polymer electrolyte and enabled solid electrochemical capacitors. *Electrochim. Acta* **2013**, *103*, 174−178.
(35) Lewandowski, A.; Świderska, A. New composite solid electrolytes based on a polymer and ionic liquids. *Solid State Ionics* **2004**, *169*, 21−24.
(36) Ortega, P. F. R.; Trigueiro, J. P. C.; Silva, G. G.; Lavall, R. L. Improving supercapacitor capacitance by using a novel gel nanocomposite polymer electrolyte based on nanostructured SiO_2, PVDF and imidazolium ionic liquid. *Electrochim. Acta* **2016**, *188*, 809−817.
(37) Li, Y.; Xiao, W.; Li, X.; Miao, C.; Guo, H.; Wang, Z. Study on performance of a novel P(VDF-HFP)/SiO_2 composite polymer electrolyte using urea as pore-forming agent. *Ionics* **2014**, *20*, 1217−1224.
(38) Shi, Y.; Fan, Z.; Ding, B.; Li, Z.; Lin, Q.; Chen, S.; Dou, H.; Zhang, X. Atomic-scale Al_2O_3 modified PEO-based composite polymer electrolyte for durable solid-state Li − S batteries. *J. Electroanal. Chem.* **2021**, *881*, 114916.
(39) Kumar, S.; Manikandan, V. S.; Palai, A. K.; Mohanty, S.; Nayak, S. K. Fe_2O_3 as an efficient filler in PVDF-HFP based polymeric electrolyte for dye sensitized solar cell application. *Solid State Ionics* **2019**, *332*, 10−15.
(40) Patel, S.; Kumar, R. Synthesis and characterization of magnesium ion conductivity in PVDF based nanocomposite polymer electrolytes disperse with MgO. *J. Alloys Compd.* **2019**, *789*, 6−14.
(41) Li, H.; Yang, J.; Xu, Z.; Lu, H.; Zhang, T.; Chen, S.; Wang, J.; NuLi, Y.; Hirano, S.-i. Integrated Composite Polymer Electrolyte Cross-Linked with SiO_2-Reinforced Layer for Enhanced Li-Ion Conductivity and Lithium Dendrite Inhibition. *ACS Appl. Energy Mater.* **2020**, *3*, 8552−8561.
(42) Nakhanivej, P.; Rana, H. H.; Kim, H.; Xia, B. Y.; Park, H. S. Transport and Durability of Energy Storage Materials Operating at High Temperatures. *ACS Nano* **2020**, *14*, 7696−7703.
(43) Lim, J. Y.; Kang, D. A.; Kim, N. U.; Lee, J. M.; Kim, J. H. Bicontinuously crosslinked polymer electrolyte membranes with high ion conductivity and mechanical strength. *J. Membr. Sci.* **2019**, *589*, 117250.
(44) Han, Y. K.; Cheon, J. Y.; Kim, T.; Lee, S. B.; Kim, Y. D.; Jung, B. M. A chemically bonded supercapacitor using a highly stretchable and adhesive gel polymer electrolyte based on an ionic liquid and epoxy-triblock diamine network. *RSC Adv.* **2020**, *10*, 18945−18952.
(45) Xie, Z.; Wu, Z.; An, X.; Yoshida, A.; Wang, Z.; Hao, X.; Abudula, A.; Guan, G. Bifunctional ionic liquid and conducting ceramic co-assisted solid polymer electrolyte membrane for quasi-solid-state lithium metal batteries. *J. Membr. Sci.* **2019**, *586*, 122−129.
(46) Zhang, J.; Zhao, N.; Zhang, M.; Li, Y.; Chu, P. K.; Guo, X.; Di, Z.; Wang, X.; Li, H. Flexible and ion-conducting membrane electrolytes for solid-state lithium batteries: Dispersion of garnet nanoparticles in insulating polyethylene oxide. *Nano Energy* **2016**, *28*, 447−454.
(47) Zhang, S.; Pan, N. Supercapacitors Performance Evaluation. *Adv. Energy Mater.* **2015**, *5*, 1401401.

https://doi.org/10.1021/acsomega.1c01623
ACS Omega 2021, 6, 16924−16933